G. Gori, D. Vimercati, A. Guardone
Non-Ideal Compressible-Fluid Effects in Oblique Shock Waves
Journal of Physics: Conference Series, Vol. 821, N. 1, 2017, 012003 (10 pages)
doi:10.1088/1742-6596/821/1/012003

IOP Conf. Series: Journal of Physics: Conf. Series **821** (2017) 012003 doi:10.1088/1742-6596/821/1/012003

Non-ideal compressible-fluid effects in oblique shock waves

G. Gori, D. Vimercati and A. Guardone

[1] Department of Aerospace Science and Technology, Politecnico di Milano
Via La Masa 34, 20156, Milano, Italy

E-mail: alberto.guardone@polimi.it

Abstract. The non-monotone dependence of the speed of sound along adiabatic transformations is demonstrated to result in the admissibility of non-ideal increase of the flow Mach number across oblique shock waves, for pre-shock states in close proximity of the liquid-vapour saturation curve. This non-ideal behaviour is primarily associated with a less-than-unity value of the fundamental derivative of gasdynamics and, therefore, non-ideal shock waves are expected to be observed in flows of fluids with moderate molecular complexity. The simple yet qualitatively sound van der Waals model is used to confirm the present findings and to provide exemplary non-ideal shock waves.

1. Introduction

The gasdynamics of single-phase flows of molecularly complex fluids in close proximity of the liquid-vapour equilibrium, for pressures on the order of those corresponding to the critical point, can significantly differ from its dilute-gas counterpart. The dynamic behaviour of compressible-fluid flows is determined by the so-called fundamental derivative of gasdynamics Γ, see reference [1], namely

$$\Gamma \equiv 1 + \rho c \left(\frac{\partial c}{\partial P} \right)_s , \tag{1}$$

where ρ is the fluid density, P the pressure, c the speed of sound and s the specific entropy. The fundamental derivative plays a central role in delineating the qualitative behaviour of fluid flows in many contexts, including, for instance, shock formation in unsteady flows, steady isentropic flow, steady duct flow with friction and steady oblique shock waves, which is the focus of the present work [1, 2, 3, 4, 5].

Conventional treatments of gasdynamics assume, either explicitly or implicitly, that $\Gamma > 1$. This is the case, for instance, for the ideal gas model, for which the fundamental derivative is a constant larger than unity. From the qualitative point of view, the behaviour of any fluid with constant $\Gamma > 1$ resembles that of ideal gases, see for instance reference [6]. It is well-known, however, that fluids with moderately or highly complex molecular structure exhibit non-ideal gasdynamic behaviour in a finite vapour-phase thermodynamic region [2, 3, 1, 7, 8]. In the non-ideal fluid-dynamic context, it is standard practice to distinguish between the cases $\Gamma \leq 0$ and $0 < \Gamma \leq 1$. In the former case, one rather speaks of non-classical gasdynamics, as opposed to classical gasdynamics if $\Gamma > 0$, because unconventional phenomena such as expansion shocks, isentropic compression fans, split shocks and composite waves are allowed, see for instance

references [1, 8, 9, 10, 11, 12, 13]. In the present work, however, the discussion will be limited to the non-ideal classical case, namely $0 < \Gamma \leq 1$, where shock waves are of the ordinary compressive type and isentropic fans carry an expansion.

Among the other effects, the non-ideal increase of the speed of sound upon isentropic expansion has important consequences on the variation of thermodynamic quantities, such as the speed of sound, along the Hugoniot locus of a given initial state, i.e. the locus of states that can possibly be connected to the initial state by means of a shock wave. The aim of this work is to provide evidence that the non-monotone dependence of the speed of sound along the Hugoniot locus can result in the non-ideal increase of the flow Mach number across oblique shock waves. The simple van der Waals model, which gives a qualitatively accurate description of the fluid behaviour in the thermodynamic region of interest in this investigation, is used for the purpose.

The characterisation of non-ideal compressible-fluid flows is not only of theoretical interest, but also is relevant to applications involving molecularly complex fluids in their dense-gas regime, such as machinery operating in Organic Rankine Cycle (ORC) and supercritical CO_2 power systems, turbogenerators, refrigerators and many others, see reference [14, 15, 16, 17]

The present work is organised as follows. In section 2, the Rankine-Hugoniot jump relations across surfaces of discontinuity are recalled along with the admissibility requirements. Exemplary oblique shock configurations for the van der Waals model of siloxane fluid MDM, are presented and discussed in section 3. Section 4 presents a numerical assessment of non-ideal streaming flows over a wedge, using the open-source CFD solver SU2, which was recently extended to deal with non-ideal thermodynamics. Section 5 presents the concluding remarks.

2. Jump relations and shock admissibility

The Euler equations of gasdynamics admit solutions including finite jumps across vanishing-thickness layers, namely surfaces of discontinuity. In a coordinate system moving with the local velocity of the discontinuity, the relations expressing the conservation of mass, momentum and energy locally assume the form

$$[\rho u_n] = 0, \tag{2a}$$
$$[\rho u_n \boldsymbol{u}_t] = 0, \tag{2b}$$
$$[P + \rho u_n^2] = 0, \tag{2c}$$
$$[\rho u_n h^t] = 0, \tag{2d}$$

where $[X] = X_B - X_A$ denotes the difference between a quantity evaluated at the post-shock state (subscript B) and at the pre-shock state (subscript A). In the above expressions, u_n is the normal component of the the velocity vector $\boldsymbol{u}$ and $\boldsymbol{u}_t$ is the tangential velocity vector, both with respect to the surface of discontinuity, and $h^t = h + u^2/2$ is the total enthalpy, where h is the fluid enthalpy and u is the magnitude of the velocity. System (2) represents the well-known Rankine-Hugoniot jump relations linking the states across a surface of discontinuity. Discontinuities having nonzero mass flux $j = \rho u_n$ are referred to as shock waves (in contrast to contact discontinuities, for which $j = 0$) and are the case of interest in this work. The Rankine-Hugoniot relations require that the tangential velocity and the total enthalpy are constant across shock waves (in the coordinate system in which the jump relations assume the form (2)). System (2) can be rearranged to obtain a single scalar equation involving the pre-shock pressure P_A and specific volume v_A and the post-shock specific volume v_B, namely

$$h(P_B, v_B) - h(P_A, v_A) - \tfrac{1}{2}(P_B - P_A)(v_B + v_A) = 0. \tag{3}$$

The above equation determines the locus of thermodynamic states that can be connected by a shock wave. Setting a generic post-shock state $P = P_B$ and $v = v_B$, the curve $P^{\mathrm{RH}}(v; P_A, v_A)$

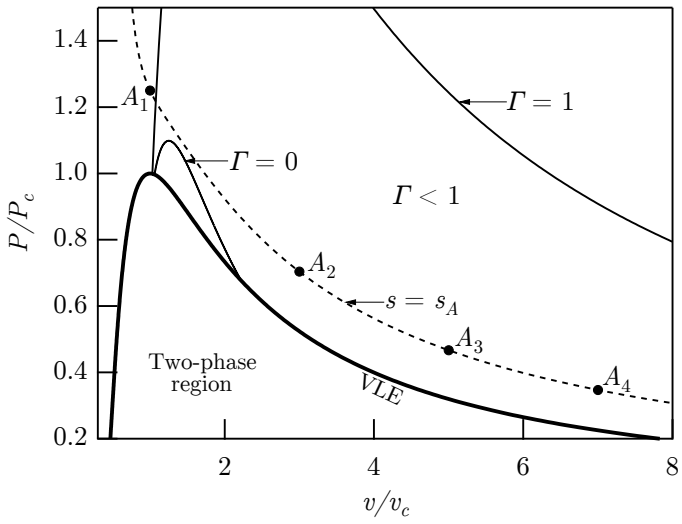

Figure 1: Pressure versus specific volume diagram computed from the polytropic van der Waals model of siloxane fluid MDM, illustrating the thermodynamic regions $\Gamma < 1$ and $\Gamma < 0$. Also shown are the four pre-shock states of the exemplary oblique shock configurations, chosen along the isentrope $s = s_A$.

defined by equation (3) is known as the *shock adiabat* centered on state A. Moreover, equations (2a) and (2c) may be combined to give

$$-\frac{P_B - P_A}{v_B - v_A} = j^2. \tag{4}$$

If the pre-shock state is fixed, and so is j^2, then the above expression defines a straight line $P^{\mathrm{R}}(v; P_A, v_A, u_{An})$, in the P-v plane, referred to as *Rayleigh line* centered on state A. The intersections between the shock adiabat and the Rayleigh line correspond to values of the post-shock specific volume that satisfy (2).

System (2) must be supplemented with admissibility criteria that exclude the unphysical solutions. By the second law of thermodynamics, the jump of the specific entropy across a shock wave must not be negative:

$$[s] \geq 0. \tag{5}$$

In addition, admissible shocks must satisfy the condition

$$M_{A,n} \geq 1 \geq M_{B,n}, \tag{6}$$

where additional subscritp n indicates the normal component, which is known as speed-ordering relation and ensures that the shock front is stable, see [18, 19]. On a geometrical basis, fulfilment of condition (6) requires

$$\left.\frac{dP^{RH}}{dv}\right|_A \geq \left.\frac{dP^{R}}{dv}\right|_A \quad \text{and} \quad \left.\frac{dP^{RH}}{dv}\right|_B \leq \left.\frac{dP^{R}}{dv}\right|_B. \tag{7}$$

As pointed out in reference [20], the entropy inequality and the speed ordering condition are sufficient to rule out inadmissible shock waves if the shock adiabat is convex, insofar as both criteria can be simultaneously satisfied only by compression ($[P] > 0$) shocks.[1]

[1] The shock adiabat is convex in the P-v plane as a direct consequence of $\Gamma > 0$. The proof, see [20], relies on the impossibility of the existence of acoustic points (at which the Rayleigh line is tangent to the shock adiabat) along the shock adiabat for $[v] \neq 0$.

Case	M_A	P_A/P_c	ρ_A/ρ_c	T_A/T_c	Γ_A
A_1	2	1.250	1.000	1.063	1.674
A_2	2	0.704	0.333	1.037	0.667
A_3	2	0.467	0.200	1.027	0.829
A_4	2	0.347	0.143	1.021	0.887

Table 1: Pre-shock states of the exemplary oblique shock configurations for the polytropic van der Waals model of siloxane fluid MDM. All the cases considered have the same pre-shock Mach number $M_A = 2$ and pre-shock entropy $s_A = s(1.250P_c, v_c)$, where subscript c denote the properties at critical point.

3. Non-ideal Oblique Shock-waves

In this section, we discuss non-ideal gasdynamic effects in steady oblique shock waves, such as those generated in a streaming steady flow over a wedge. The wedge prescribes a flow deflection angle $\theta \leq \theta_{\max}$, which is realized by a planar shock wave of angle β which originates from the corner and separates the two uniform regions A and B, upstream and downstream of the shock, respectively. The condition $\theta = \theta_{max}$ corresponds to the maximum deflection that the flow can sustain across a planar attached shock wave. If $\theta > \theta_{\max}$, the shock wave detaches and it is no longer a planar front.

The following treatment is intended to provide evidence of non-ideal gasdynamic effects across planar shock waves in flows of fluids experiencing $0 < \Gamma \leq 1$. Exemplary cases will be investigated in which the magnitude of the Mach number increases as the flow passes through the shock wave, namely $M_B > M_A$. From the theoretical point of view, this is possible in any fluid flow in the regime $\Gamma < 1$, because the speed of sound no longer increases monotonically with increasing density along the shock adiabat. As a result, the magnitude of the tangential component of the Mach number may possibly increase, and such an increase may not be compensated by the necessary decrease in the normal Mach number. The latter claim is confirmed in the following by means of the polytropic (i.e., with constant isochoric specific heat c_v) van der Waals model [21], which is one of the simplest, yet qualitatively correct, thermodynamic models allowing for a non-constant Γ. As pointed out by Kluwick [22], the condition $c_v/R \gtrsim 3.78$ is to be satisfied in order that a thermodynamic region featuring $\Gamma < 1$ exists in the vapor phase. Figure 1 shows a portion of the non-ideal thermodynamic region $\Gamma < 1$ for the polytropic van der Waals model of siloxane fluid MDM (corresponding to $c_v/R = 57.69$), which will be used throughout the present work, together with the nonclassical region $\Gamma < 0$. The present investigation will be limited to oblique shocks that exhibit non-ideal, yet classical, features. Therefore, we will naturally focus on shock waves whose adiabat lies entirely in the region $\Gamma > 0$. The analysis of steady oblique shock waves in the regime of mixed nonlinearity, where nonclassical wave fields are expected to occur [1, 8, 12], is left for future investigations.

A set of exemplary cases for the polytropic the van der Waals model of siloxane fluid MDM is examined and used to investigate the dependence of the properties of oblique shock waves on the upstream state (P_A, v_A, M_A). Four different upstream states are considered, as described in table 1 and shown in figure 1. In order to simplify the following treatment, the selected configurations exhibit the same upstream values of the Mach number and of the entropy, namely $M_A = 2$ and $s_A = s(1.25P_c, v_c)$. Firstly, we consider oblique shocks originating form pre-shock state A_1, which is located in the region $\Gamma > 1$ at density values higher than those corresponding to $\Gamma < 1$. Hence, $\Gamma_{A_1} > 1$ and, with reference to figure 2a, the compressive branch of shock adiabat H_1 centred on state A_1 is entirely located in the region $\Gamma > 1$. The endpoint denoted as N_1 corresponds the post-shock state of the normal shock from state A_1. Figure 3a shows the variation of the ratios c_A/c_B, M_B/M_A and $M_{B,n}/M_{A,n}$ with the shock angle β. Owing to relation (2b), the tangential component of the velocity (with respect to the oblique shock) is conserved across the shock and, therefore, $c_A/c_B = M_{B,t}/M_{A,t}$, where the additional subscript

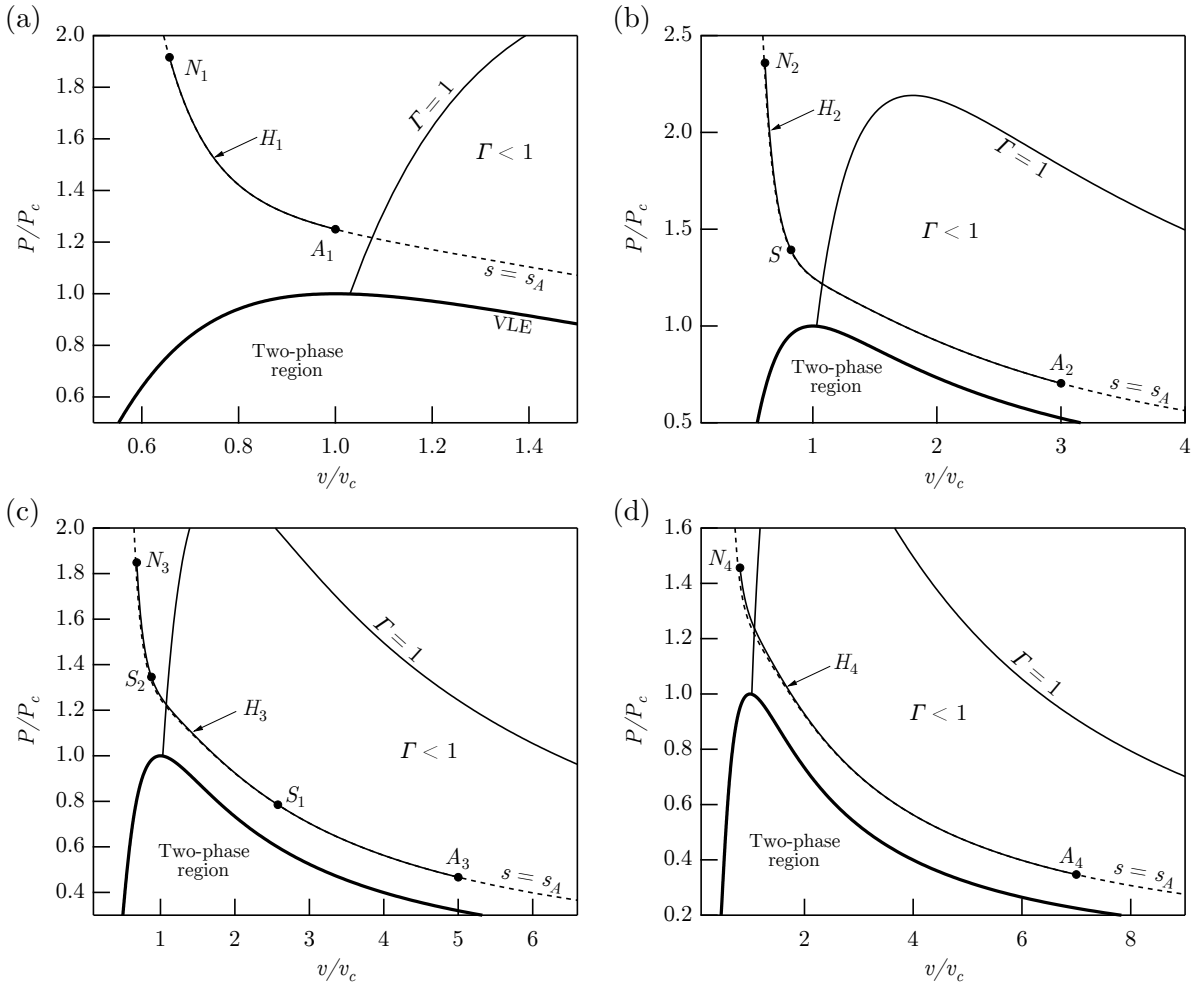

Figure 2: Pressure versus specific volume diagrams illustrating shock adiabats (curves labelled H) originating from pre-shock states corresponding to (a) case A_1, (b) case A_2, (c) case A_3 and (d) case A_4, as computed from the polytropic van der Waals model of siloxane fluid MDM. The endpoints labelled as N correspond to the normal shock configuration. Also shown are the post-shock states S at which $M_B = M_A$.

t denotes the tangential component. The range of shock angles spans from the minimum value $\beta_{\min} = \text{asin}(1/M_A)$, corresponding to an acoustic wave, up to $\beta = \pi/2$, corresponding to a normal shock wave. Note that β may also be used to parametrize the shock adiabat in place of v (except for the trivial shock $[v] = 0$ and $M_{B,n} = 1$), because

$$dv = 2\text{cotg}\beta \frac{M_{B,n}^2}{1 - M_{B,n}^2} \left(1 + \frac{[v]}{2v_B} G_B\right) [v] d\beta,$$

where $G = v(\partial P/\partial e)_v$ is the Gruneisen parameter and condition $1 + [v]G_B/(2v_B) = 0$ is the singularity that limits the maximum density increase across compressive shock waves, see for instance Kluwick [23]. Hence, along the compressive branch of the shock adiabat, the post-shock specific volume decreases with increasing shock angle. As shown in figure 3a, c_B increases and, therefore, $M_{B,t}/M_{A,t}$ decreases with increasing β or, equivalently, decreasing v. Because $M_{B,n} < M_{A,n}$ as required by the speed ordering relation, $M_B < M_A$ for each possible oblique

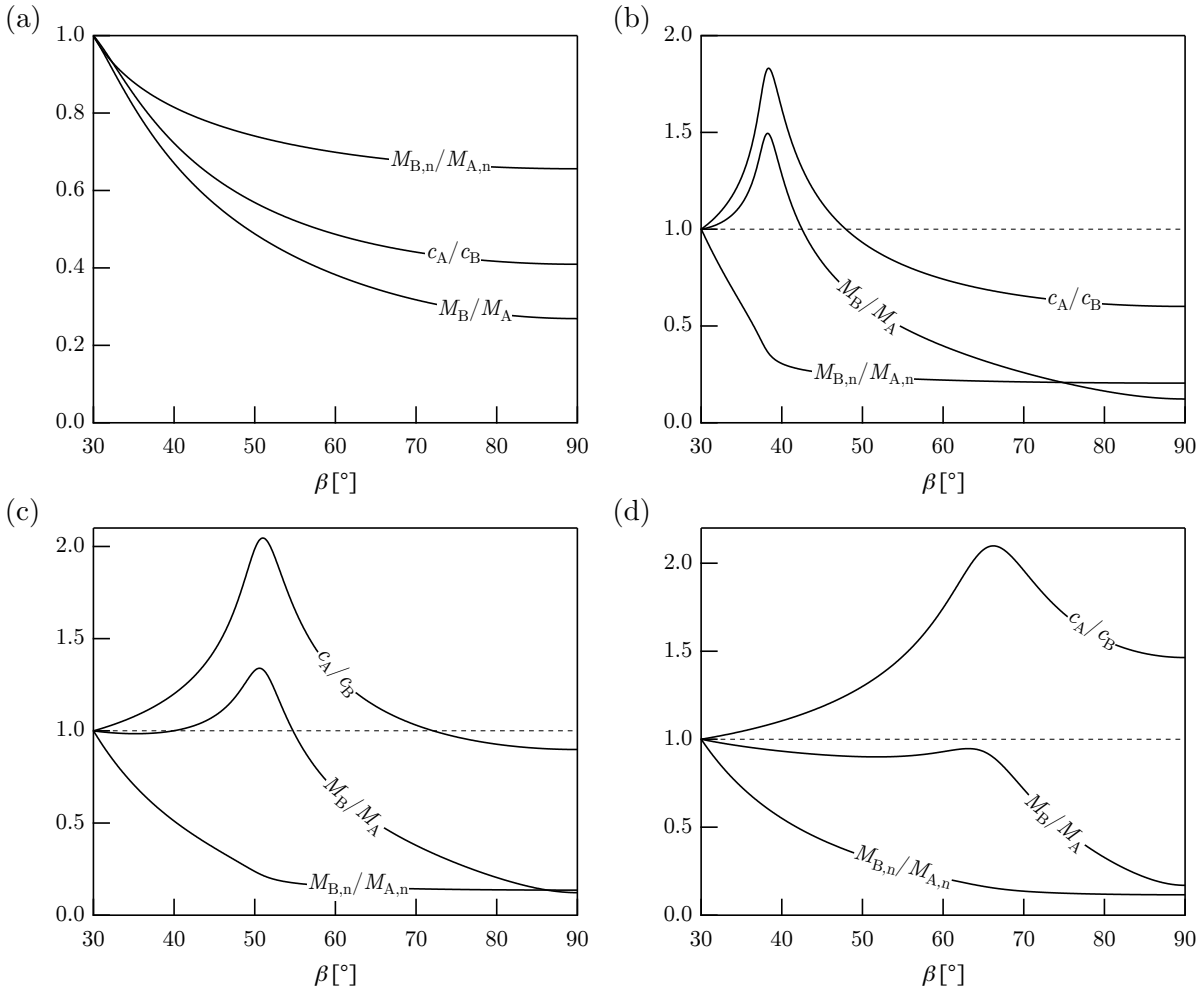

Figure 3: Variation of the speed of sound ratio c_A/c_B, normal Mach number ratio $M_{B,n}/M_{A,n}$ and Mach number ratio M_B/M_A with shock angle β for (a) case A_1, (b) case A_2, (c) case A_3 and (d) case A_4, as computed from the polytropic van der Waals model siloxane fluid MDM. The shock angle spans from the minimum value $\beta = \mathrm{asin}(1/M_A)$, corresponding to an acoustic wave, up to the maximum value $\beta = \pi/2$, corresponding to a normal shock wave.

shock configuration with upstream state A_1. These observations could be anticipated and reasonably justified by neglecting the entropy rise across the shock wave, so that the shock adiabat would coincide with the isentrope passing through the pre-shock state. In this limit, the speed of sound would necessarily increase with increasing density because $\Gamma > 1$. However, this is true even if we take into account the entropy rise whenever condition $(\partial c/\partial s)_v > 0$ is satisfied, as it is the case within the polytropic van der Waals model. Moreover, as discussed by Menikoff and Plohr [12], $(\partial c/\partial s)_v > 0$ is expected to hold to occur for most real materials in their pure phases.

Next, state A_2, with $\Gamma_{A_2} < 1$, is considered. With reference to figure 2b, a wide portion of the shock adiabat H_2 lies inside the region $\Gamma < 1$. As is expected due to the almost negligible entropy rise together with $\Gamma_B < 0$, c_B initially decreases with increasing shock angle, as shown in figure 3b, where $c_B < c_A$ up to 47.9° and a pronounced local minimum if found at 38.3°. As a result, there exists a range of shock angles in which the increase in tangential component of the Mach number is sufficient to compensate the necessary decrease in the normal Mach number.

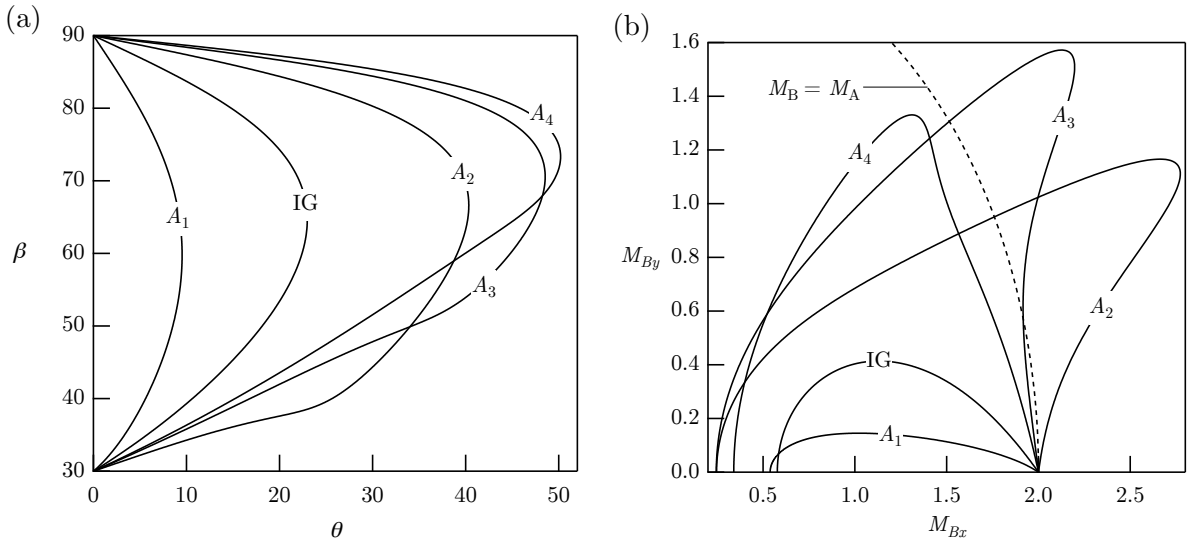

Figure 4: Diagrams illustrating (a) the variation of the flow deflection angle θ with shock angle β and (b) the polar of the Mach number, where $M_{Bx} = M_B \cos\theta$ and $M_{By} = M_B \sin\theta$, as computed from the polytropic van der Waals model of siloxane fluid MDM. Also shown are the curves, labeled IG, that correspond to the polytropic ideal gas case with the same upstream Mach number M_A used in the computation of the non-ideal cases.

The post-shock state characterized by $M_B = M_A$ occurs at 42.5° and it is denoted as point S in figure 2b. In the range between $\beta = \beta_{\min}$ and $\beta = 42.5°$ the post-shock Mach number exceeds the pre-shock Mach number. The local peak in the post-shock Mach number is found at 38.2° and corresponds to the ratio $M_B/M_A = 1.5$.

If the pre-shock density is further lowered, a larger portion of the shock adiabat in embedded in the region $\Gamma < 1$, as shown in figure 2c for the case corresponding to pre-shock state A_3. As a result, the range of shock angles where $c_B < c_A$ also increases, see 3c. For the present configuration, $c_B < c_A$ up to 72.1° with a local maximum at 51.0°. However, the evolution of the Mach number is somewhat more complex if compared to the previous case. The Mach number initially decreases with increasing shock angle, as the increase of $M_{B,t}$ is overcompensated by the decrease of $M_{B,n}$. At $\beta = 35.2°$, the post-shock Mach number shows a local minimum and subsequently increases up to the pronounced peak ($\beta = 50.6°$) associated with the local minimum in the post-shock speed of sound. The two post-shock states that satisfy $M_B = M_A$ are shown in figure 2c, where they are denoted as points S_1 and S_2. State S_1 corresponds to a shock angle $\beta = 39.8°$ and it is located inside the region $\Gamma < 1$; post-shock state S_2 occurs at $\beta = 54.7°$ and, similarly to state S of case A_2, it is located in the thermodynamic region $\Gamma > 1$.

In our last exemplary case, we consider pre-shock state A_4. With reference to figure 2d, the shock adiabat H_4 is almost entirely embedded in the region $\Gamma < 1$ and, as a result, $c_B < c_A$ over the complete range of shock angles, as shown in 3d. However, the local minimum in the post-shock speed of sound now occurs at such large values of β that the necessary decrease in the normal component of the Mach number across the shock wave is sufficient to compensate the non-ideal increase in the tangential component of the Mach number. Therefore, $M_B < M_A$ for each possible oblique shock configuration originating from state A_4.

The variation of the flow deflection angle θ with the shock angle β for each of the configurations considered is shown in figure 4a, where it is compared with the curve labelled IG, that corresponds to the polytropic ideal gas case and, as is well-known, is independent of the

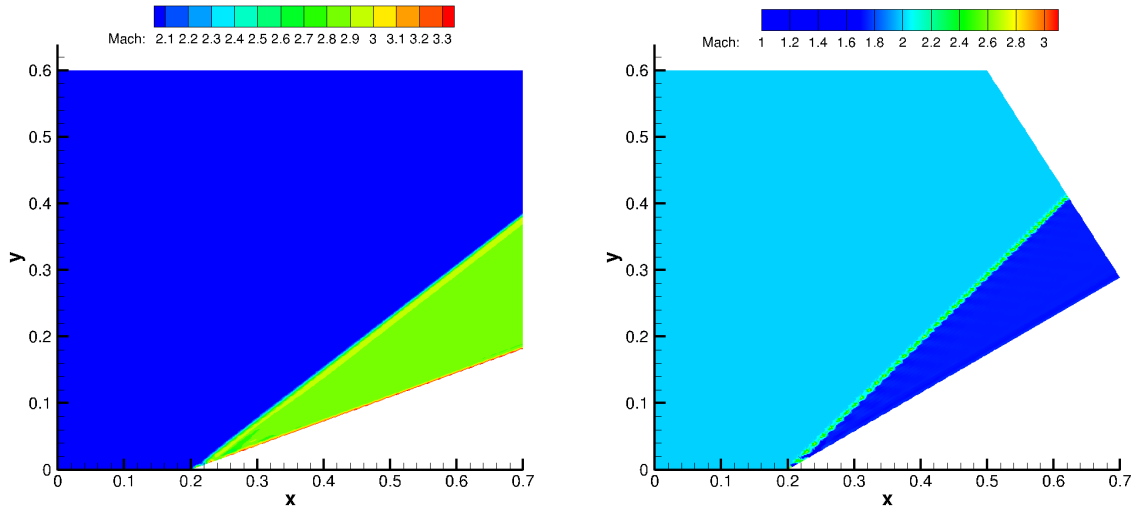

Figure 5: Left picture shows the computed Mach number field for a turning angle of $\theta = 20°$, while right picture presents the same result for a turning angle of $\theta = 30°$.

pre-shock thermodynamic state P_A, v_A [6]. The curves computed by means of the polytropic van der Waals model exhibit substantial differences depending on the pre-shock thermodynamic state. In particular, the maximum turning angle $\theta_{\max}$ that the flow can sustain across a planar attached shock waves varies from 9.5° of case A_1 up to 50.2° of case A_4. In contrast, $\theta_{\max} = 23.0°$ for the polytropic ideal gas.

Finally, the same results can be conveniently presented also in term of the shock polar for the Mach number, namely a plot of $M_{By} = M_B \sin\theta$ versus $M_{Bx} = M_B \cos\theta$, as shown in figure 4b for each non-ideal configuration considered and the polytropic ideal gas counterpart.

4. Numerical Results

In this section numerical simulations are reported to illustrate exemplary flow conditions, chosen among those discussed in the previous, theoretical section. Numerical simulations were run using SU2, an open-source Computational Fluid Dynamic (CFD) solver, which was recently extended to non-ideal and non-classical flows [24]. SU2 contains an embedded thermodynamic library which counts several different equation of state but can also exploit external library such as FluidProp. In the numerical simulations presented hereinafter only the polytropic van der Waals equation of state was considered, so that they can be compared to the results presented in the previous sections. In figure 5, exemplary computed flow fields for a turning angle of $\theta = 20°$, on the left-hand side, and $\theta = 30°$, on the right side, are reported. The flow enters the domain at left vertical boundary, where the state A_2 (with reference to table 1) is prescribed, and exits through the right boundary at supersonic speed. On the upper and lower boundaries an inviscid wall condition is imposed. The domain for the higher value of turning angle has a non-vertical outlet boundary to help the convergence of the numerical simulation. Both picture clearly show the presence of a shock-wave induced by the slope discontinuity at the lower all. Note that in the numerical simulations, an artificial internal shock structure is formed in which overshoots of the flow variables are observed. These are numerical artefacts common to all shock-capturing methods.

Figure 6 shows reduced density and pressure values for a fluid entering the domain at conditions A_2, taken along a horizontal line crossing the domain at $y = 0.2$. From figure 6 it is possible to verify that density and pressure increase for each different value of turning

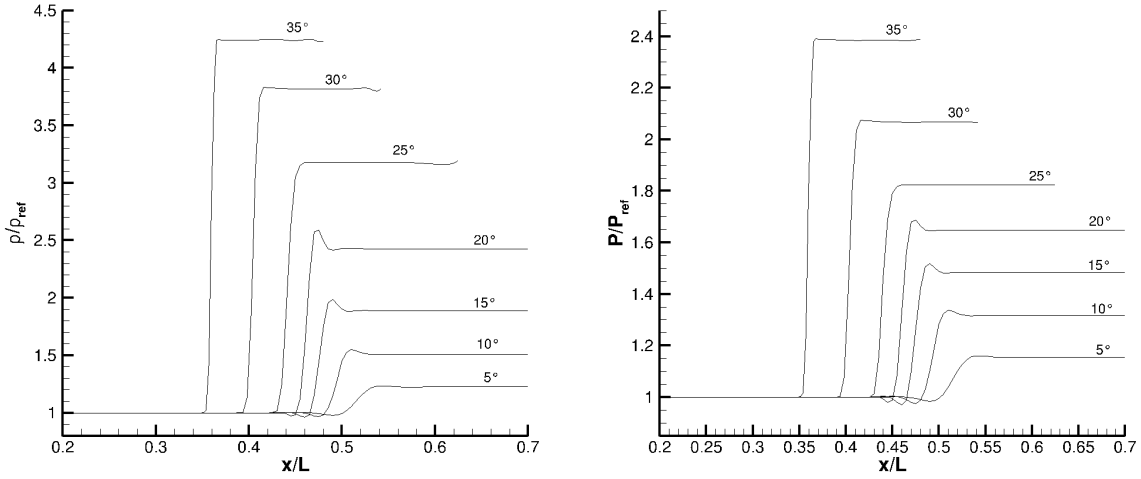

Figure 6: Left picture shows reduced density values ($\rho_{\text{ref}} = 85.6067$ kg/m^3) while right picture shows the pressure ($P_{\text{ref}} = 996220$ Pa) trends for several, different, turning angles. The density and pressure profiles were extracted along a line crossing the domain at $y = 0.2$.

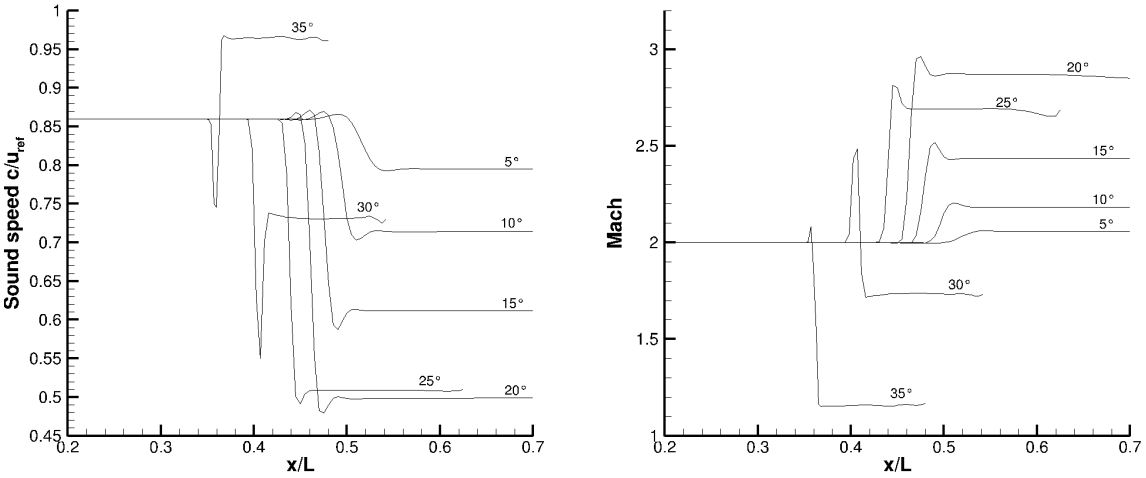

Figure 7: Left picture shows reduced speed of sound values ($u_{\text{ref}} = 107.876$ m/s) while right picture shows the Mach trends for several, different, turning angles. The speed-of-sound and Mach profiles were extracted along a line crossing the domain at $y = 0.2$.

angle. This means that the shock maintains its compressive nature and the flow can be still categorised as non-ideal. In figure 7, speed of sound and Mach number trends are reported. From this graph it is possible to observe the non-ideal effect causing the Mach number to rise through an oblique shock-wave, in agreement with theoretical predictions. For this particular pre-shock thermodynamic state A_2, non-ideal phenomena are revealed in numerical simulations for a set turning angle which spans from 5 to 25 degrees. The highest M_B/M_A ratio is reached at $\theta = 20°$ while for $\theta = 30°$ and $\theta = 35°$ the flow does not present unusual features, as predicted by theory.

5. Conclusions

Steady oblique shock waves were investigated in the non-ideal thermodynamic framework. It was shown that, if the pre-shock state is located in close proximity of the non-ideal thermodynamic region $\Gamma < 1$, the speed of sound need not increase with pressure along the shock adiabat. The exemplary computations were performed using the polytropic van der Waals model of siloxane fluid MDM, for which the post-shock Mach number was found to increase up to 1.5 times the pre-shock Mach number. The present analysis has a sound theoretical basis, owing to the fact that simple van der Waals model is known to predict the correct qualitative behaviour in the single-phase thermodynamic region close to liquid-vapour equilibrium (sufficiently far from the critical point for critical phenomena to be negligible). Therefore, non-ideal shock waves are expected to be predicted also by more complex thermodynamic models, such as the Peng-Robinson [25], the Martin-Hou [26, 27] or the Span-Wagner [28, 29]. A more complete study is left for future investigations. The experimental verification of the occurrence of non-ideal shock waves can be devised in test rigs working with fluids of high or even moderate molecular complexity, though certain practical difficulties, mostly related to thermal stability of the working fluid, may be raised. Future work includes the definition of the thermodynamic admissibility region for non-ideal shock waves and the extension to flows of fluids exhibiting negative nonlinearity.

6. References

[1] Thompson P A 1971 *Phys. Fluids* **14** 1843–1849
[2] Bethe H A 1942 The theory of shock waves for an arbitrary equation of state Technical paper 545 Office Sci. Res. & Dev.
[3] Zel'dovich Y B 1946 *Zh. Eksp. Teor. Fiz.* **4** 363–364
[4] Weyl H 1949 *Comm. Pure Appl. Math.* **2** 103–122
[5] Hayes W D 1958 *Fundamentals of gasdynamics* (*High speed aerodynamics and jet propulsion* vol 3) ed Emmons H W (Princeton, N.J.: Princeton University Press) pp 416–481
[6] Thompson P A 1988 *Compressilbe Fluid Dynamics* (McGraw-Hill)
[7] Lambrakis K C and Thompson P A 1972 *Phys. Fluids* **15** 933–935
[8] Thompson P A and Lambrakis K C 1973 *J. Fluid Mech.* **60** 187–208
[9] Cramer M S and Kluwick A 1984 *J. Fluid Mech.* **142** 9–37
[10] Cramer M S and Sen R 1986 *Phys. Fluids* **29** 2181–2191
[11] Cramer M S and Sen R 1987 *Phys. Fluids* **30** 377–385
[12] Menikoff R and Plohr B J 1989 *Rev. Mod. Phys.* **61(1)** 75–130
[13] Bates J W and Montgomery D C 1999 *Phys. Fluids* **11** 462–475
[14] Colonna P, Harinck J, Rebay S and Guardone A 2008 *J. Propul. Power* **24** 282–294
[15] Congedo P, Corre C and Cinnella P 2011 *Comput. & Fluids* **49** 290–301
[16] Wheeler A and Ong J 2013 *J. Eng. Gas Turbines Power* **135** 102603
[17] Colonna P, Casati E, Trapp C, Mathijssen T, Larjola J, Turunen-Saaresti T and Uusitalo A 2015 *J. Eng. Gas Turb. Power* **137** 100801–1–19
[18] Lax P D 1957 *Commun. Pur. Appl. Math.* **10** 537–566
[19] Oleinik O 1959 *Usp. Mat. Nauk* **14** 165–170
[20] Landau L D and Lifshitz E M 1987 *Fluid mechanics, 2nd edn* (Pergamon Press)
[21] van der Waals J D 1873 *Over de Continuïteit van den Gas - en Vloeistoftoestand (on the continuity of the gas and liquid state)* Ph.D. thesis Leiden University
[22] Kluwick A 2004 *Acta Mech.* **169** 123–143
[23] Kluwick A 2001 *Handbook of Shock Waves* (Academic Press) chap 3.4. Rarefaction shocks, pp 339–411
[24] Vitale S, Gori G, Pini M, Guardone A, Economon T D, Palacios F, Alonso J J and Colonna P 2015 *AIAA Paper* **2760**
[25] Peng D Y and Robinson D B 1976 *Ind. Eng. Chem. Fundam.* **15** 59–64
[26] Martin J J and Hou Y C 1955 *AIChE J.* **1** 142–151
[27] Martin J J, Kapoor R M and De Nevers N 1959 *AIChE J.* **5** 159–160
[28] Span R and Wagner W 2003 *Int. J. Thermophys.* **24** 1–39
[29] Span R and Wagner W 2003 *Int. J. Thermophys.* **24** 41–109